Normal Gas-Rich Galaxies in the Far-Infrared: The Legacy of ISOPHOT

Richard J. Tuffs & Cristina C. Popescu

Max Planck Institut für Kernphysik, Astrophysics Department,
Saupfercheckweg 1, D-69117 Heidelberg,
e-mail:Richard.Tuffs@mpi-hd.mpg.de; Cristina.Popescu@mpi-hd.mpg.de

Abstract. Following on from IRAS, the ISOPHOT instrument on board the Infrared Space Observatory (ISO) has provided a huge advancement in our knowledge of the phenomenology of the far-infrared (FIR) emission of normal galaxies and the underlying physical processes. Highlights include: the discovery of an extended cold dust emission component, present in all types of gas-rich galaxies and carrying the bulk of the dust luminosity; the definitive characterisation of the spectral energy distribution in the FIR, revealing the channels through which stars power the FIR light; the derivation of realistic geometries for stars and dust from ISOPHOT imaging and the discovery of cold dust associated with HI extending beyond the optical body of galaxies.

1. INTRODUCTION

Whereas IRAS provided the first systematic survey of far-infrared (FIR) emission from normal galaxies, it has been the photometric, imaging and spectroscopic capabilities of the ISOPHOT instrument (Lemke et al. [51]) on board the Infrared Space Observatory (ISO; Kessler et al. [47]) which have unravelled the basic physical processes giving rise to this FIR emission. Thanks to the broad spectral grasp of ISOPHOT, the bulk of the emission from dust could be measured, providing the first quantitative assessment of the fraction of stellar light re-radiated by dust. The battery of filters has led to a definitive characterisation of the spectral energy distribution (SED) in the FIR, revealing the contribution of the different stellar populations in powering the FIR emission. The imaging capabilities have unveiled the complex morphology of galaxies in the FIR, and their changing appearance with FIR wavelength. They also allowed the exploration of hitherto undetected faint diffuse regions of galaxies.

In this review we will concentrate on the FIR properties of normal nearby galaxies. By normal we essentially mean that their SEDs are not powered by accretion. We will begin with spiral galaxies and then we will move to the other class of gas-rich galaxies, the dwarfs.

CP761, *The Spectral Energy Distributions of Gas-Rich Galaxies: Confronting Models with Data*
edited by C.C. Popescu and R.J. Tuffs

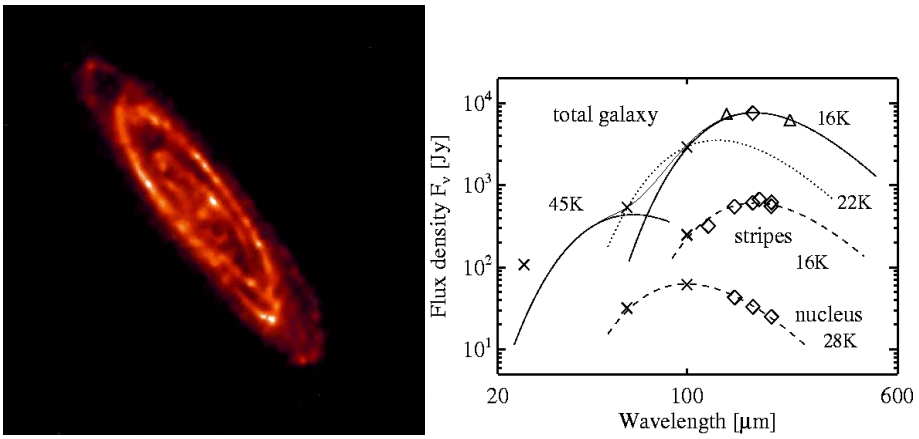

FIGURE 1. Left: ISOPHOT 170 μm map of M 31 (Haas et al. [34]), with an angular resolution of 1.3′. North is towards the top, and East is towards the left. The field size is 2.9×2.9 degrees. Right: Infrared SED of M 31 (Haas et al. [34]). The data are shown by symbols (diamonds ISO, crosses IRAS, triangles DIRBE) with the size being larger than the errors. The blackbody curves with emissivity proportional to λ^{-2} are shown by lines. The dotted line with T=22 K through the IRAS 60 and 100 μm data points indicates what one would extrapolate from this wavelength range alone without any further assumptions.

2. SPIRAL GALAXIES

2.1 Spatial distributions

2.1.1 FIR Morphologies

ISOPHOT imaged three nearby galaxies (M 31: Haas et al. [34]; M 33: Hippelein et al. [42] and M 101: Tuffs & Gabriel [86]) in the 60 to 200 μm range, with sufficient linear resolution to easily distinguish between the main morphological components in the FIR - nucleus, spiral arms and underlying disk. The main discovery, made possible by the unprecedented surface brightness sensitivity longwards of 100 μm, was the existence of large amounts of cold dust associated both with the spiral arms and with the underlying disk. This dust was too cold to have been seen by IRAS. Furthermore, ground-based submillimeter (submm) facilities have lacked the surface brightness sensitivity to map the diffuse component of the cold dust associated with the underlying disk. Recently, however, a submillimeter counterpart of the diffuse disk known from FIR studies was revealed through deep SCUBA mapping of M 51 (Meijerink et al. [58]).

In the case of the Sab galaxy M 31, most of the emission at 170 μm arises from the underlying disk, which has a completely diffuse appearance (Fig. 1, left panel). This diffuse disk emission can be traced out to a radius of 22 kpc, so the galaxy has a similar overall size in the FIR as seen in the optical bands. Fig. 1 (left panel) also shows that at 170 μm the spiral arm component is dominated by a ring of 10 kpc radius. In addition, there is a faint nuclear source, which is seen more prominently in HIRES IRAS 60 μm maps at similar resolution and in Hα. The overall SED (Fig. 1, right panel)

can be well described as a superposition of two modified (β=2) Planck curves, with dust temperatures T_D of 16 and 45 K. The cold dust component at 16 K arises from both the ring structure (30%) and the diffuse disk (70%; Haas, private communication), illustrating the importance of the diffuse emission at least for this example. The 45 K component matches up well with HII regions within the star-formation complexes in the ring structure. Associated with each star-formation complex are also compact, cold emission sources (Schmitobreick et al. [76]) with dust temperatures in the 15 to 20 K range. These could well represent the parent molecular clouds in the star-formation complexes which gave rise to the HII regions. Detailed examination of the morphology of the ring shows a smooth component of cold dust emission as well as the discrete cold dust sources. Finally, the nuclear emission was fitted by a 28 K dust component.

The ISOPHOT maps of the Sc galaxies M 33 and M 101 show the same morphological components as seen in M 31, with the difference that the spiral arm structure can be better defined in these later-type spirals. Also the star-formation complexes in the spiral arms show similar SEDs to those seen in M 31.

In conclusion, the characteristics of the FIR emission from the main morphological components of spiral galaxies are:

- **nucleus**: an unresolved warm source with $T_D \sim 30$ K
- **spiral arms**: a superposition of:
  - localised warm emission with $40 \leq T_D \leq 60$ K from HII regions
  - localised cold emission with $15 \leq T_D \leq 20$ K from parent molecular clouds
  - diffuse emission running along the arms
- **disk**: an underlying diffuse (predominantly cold) emission with $12 \leq T_D \leq 20$ K

2.1.2 The extent of spiral disks in the FIR

Further information about the distribution of dust in spiral disks is provided by FIR observations of galaxies more distant than the highly resolved local galaxies discussed in Sect. 2.1.1, but still close enough to resolve the diffuse disk at the longest FIR wavelengths accessible to ISO. In a study of eight spiral galaxies mapped by ISOPHOT at 200 μm, Alton et al. ([1]; see also Davies et al. [23] for NGC 6946) showed that the observed scalelength of FIR emission at 200 μm is greater than that found by IRAS at 60 and 100 μm. Thus, the scalelength of the FIR emission increases with increasing FIR wavelength. This result was reinforced using LWS measurements of the dust continuum by Trewhella et al. [84], and can also be inferred from Hippelein et al. [42] for M 33. This implies that the bulk of the 200 μm emission arises from grains heated by a radially decreasing radiation field, as would be expected for grains in the diffuse disk. If most of the 200 μm emission had arisen from localised sources associated with the parent molecular clouds, there should be no FIR colour gradient in the galaxy, since the SEDs of sources which are locally heated should not depend strongly on position.

The second result to come out of the studies by Alton et al. [2] and Davies et al. [23] is that the observed scalelength at 200 μm is comparable to or exceeds the scalelength of the optical emission (see also Tuffs et al. [85]). As noted by Alton et al. [2], this result implies that the *intrinsic* scalelength of the dust in galaxies is greater than that of the

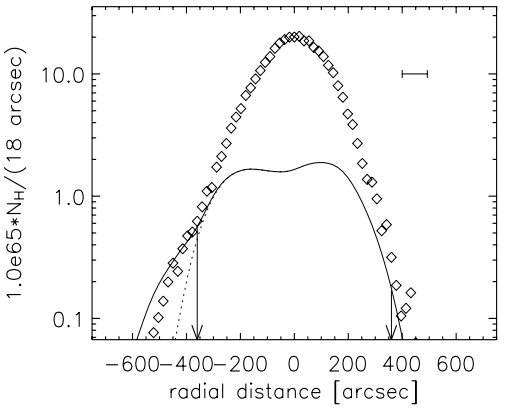

FIGURE 2. The radial profiles of HI emission (from Swaters et al. [83]) convolved with the ISOPHOT PSF (solid line) and of 200 μm FIR emission (symbols) of NGC 891 (Popescu & Tuffs [68]). Note that the extent and asymmetry of the 200 μm emission follow that of the HI emission. The profiles are sampled at intervals of 18″. The negative radii correspond to the southern side of the galaxy and the galaxy was scanned at 60 degrees with respect to the major axis. The units of the FIR profile are W/Hz/pixel, multiplied by a factor of 2×10^{-22} and the error bars are smaller than the symbols. The horizontal bar delineates the FWHM of the ISOPHOT PSF of 93″. The vertical arrows indicate the maximum extent of the optically emitting disk. The dotted line represents a modified HI profile obtained in the southern side from the original one by cutting off its emission at the edge of the optical disk and by convolving it with the ISOPHOT PSF.

stars. This is because the apparent scalelength of stars should increase with increasing disk opacity (since the inner disk is expected to be more opaque than the outer disk) whereas the apparent scalelength of the dust emission will be less than the intrinsic scalelength (due to the decrease in grain temperature with increasing galactocentric radius). The extraction of the precise relation between the intrinsic scalelengths of stars and dust requires a self-consistent calculation of the transfer of radiation through the disk (see Popescu & Tuffs [69]). The reason for the difference between the intrinsic scalelength of stars and dust in galaxies is not self-evident, since it is the stars themselves which are thought to be the sources of interstellar grains (produced either in the winds of evolved intermediate mass stars or perhaps in supernovae). One might speculate either that there is a mechanism to transport grains from the inner disk to the outer disk, or that the typical lifetimes of grains against destruction by shocks is longer in the outer disk than it is in the inner disk.

While Alton et al. and Davies et al. showed that the scalelength of the 200 μm emission was comparable to or slightly larger than that of the optical emission, these studies did not actually detect grain emission beyond the edge of the optical disk. Since spiral galaxies in the local universe are commonly observed to be embedded in extended disks of neutral hydrogen - the so called “extended HI disks”, it is a natural question to ask whether these gaseous disks contain grains. This question was answered in the affirmative by Popescu & Tuffs [68], through dedicated deep FIR maps of a large field encompassing the entire HI disk of the edge-on spiral galaxy NGC 891, made using ISOPHOT at 170 and 200 μm (see Fig. 2.).

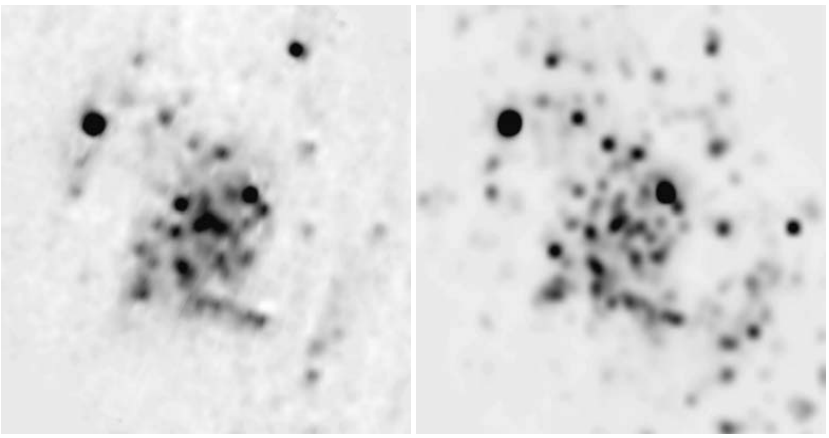

FIGURE 3. Left: Distribution of the localised warm dust component at 60 μm, F_{60}^{l}, in M 33 (Hippelein et al. [42]). This is the scaled difference map $2(F_{60} - 0.165 \times F_{160})$, with the factor 0.165 given by the average flux density ratio F_{60}/F_{170} in the interarm regions. Right: $H\alpha$ map of M 33 convolved to a resolution of 60″.

The large amounts of grains found in the extended HI disk of NGC 891 (gas-to-dust ratio of $\sim$ 1%) clearly shows that this gaseous disk is not primordial, left over from the epoch of galaxy formation. It was suggested that the detected grains could have either been transported from the optical disk (via the halo, using mechanisms such as those proposed by Ferrara [29], Davies et al. [22], Popescu et al. [70] or through the action of macro turbulence) or that they could have been produced outside the galaxy (for example transferred in interactions with other galaxies). It is interesting to note that, although the dust emission is seen towards the HI component, the grains may not actually be embedded in the neutral ISM. Instead, this dust could trace an "unseen" molecular component, as proposed by Pfenniger & Combes [63], Pfenniger, Combes & Martinet [64], Gerhard & Silk [31], and Valentijn et al. [92]. This cold molecular gas component has been invoked as a dark matter component to explain the flat rotation curves of spiral galaxies. Its presence might also reconcile the apparent discrepancy between the very low metallicities measured in HII regions in the outer disk (Ferguson, Gallagher & Wyse [28]) and the high ratio of dust to gas (on the assumption that all gas is in form of HI) found by Popescu & Tuffs [68] in the extended HI disk of NGC 891.

2.1.3 Comparison with morphologies at other wavelengths

Comparison with Hα

For the highly resolved galaxy M 33, Hippelein et al. [42] showed that there is a strong resemblance between the morphology of the localised warm dust component at 60 μm (F_{60}^{l}; obtained at each direction by subtracting the 170 μm map scaled by the ratio of the 60/170 μm brightness in the interarm regions) and the morphology of the Hα emission (see Fig. 3), indicating that the 60 μm localised emission traces the star-formation

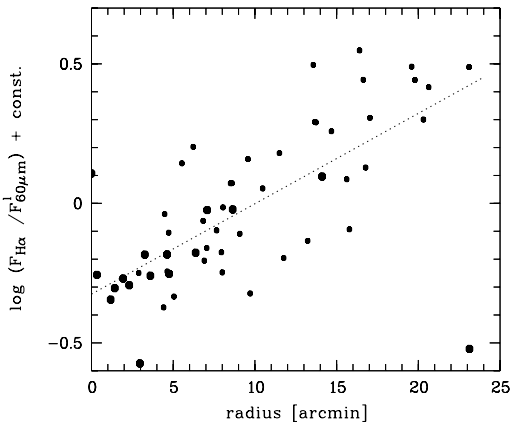

FIGURE 4. The ratio of $F_{H\alpha}$ to the localised warm dust component at 60 μm, $F^{\rm l}_{60}$, for the star-forming regions in M 33 (Hippelein et al. [42]) versus distance from the galaxy centre. Symbol sizes indicate the brightness of the sources.

complexes. The $F_{H\alpha}/F^{\rm l}_{60}$ ratio (see Fig. 4) for the star-formation complexes shows a clear systematic increase with increasing radial distance from the centre (allowing for the [NII] line contribution decreasing with distance, the slope would be even steeper). Very probably this is due to the presence of a larger scale gradient of opacity affecting the recombination line fluxes.

Comparison with UV

A fundamental property of spiral galaxies is the fraction of light from young stars which is re-radiated by dust. This property can be investigated as a function of position in the galaxy by a direct comparison of ISOPHOT maps at 60, 100 and 170 μm with UV maps obtained with GALEX (Galaxy Evolution Explorer; Martin et al. [56]) in its near-UV (NUV; 2310 Å) and far-UV (FUV; 1530 Å) bands. Such a comparison was performed for M 101 by Popescu et al. [72]. The top panels in Fig. 5 display the 100 μm ISOPHOT image (left) together with the corresponding "total UV" (integrated from 1412 to 2718 Å) image (right). Comparison between the ratio image (100 μm/UV) (bottom left panel) and an image of the "spiral arm fraction" (the fraction of the UV emission from the spiral arm within an ISOPHOT beam; bottom right panel) shows that the high values of the 100 μm/UV ratio trace the interarm regions. In other words the "spiral features" in the ratio image are in reality regions of diffuse emission which are interspaced with the real spiral features, as seen in the "spiral arm fraction" image.

The trend for the FIR/UV ratio to be higher in the diffuse interarm regions than in the spiral-arms is seen in Fig. 6 from the segregation of the blue dots and red diamonds at a given radius. This apparently surprising result was explained in terms of the escape probability of UV photons from spiral arms and their subsequent scattering in the interarm regions, and in terms of the larger relative contribution of optical photons to the heating of the dust in the interarm regions. The combined effect of the optical heating and the scattering of the UV emission means that the FIR/UV ratio will not be a good

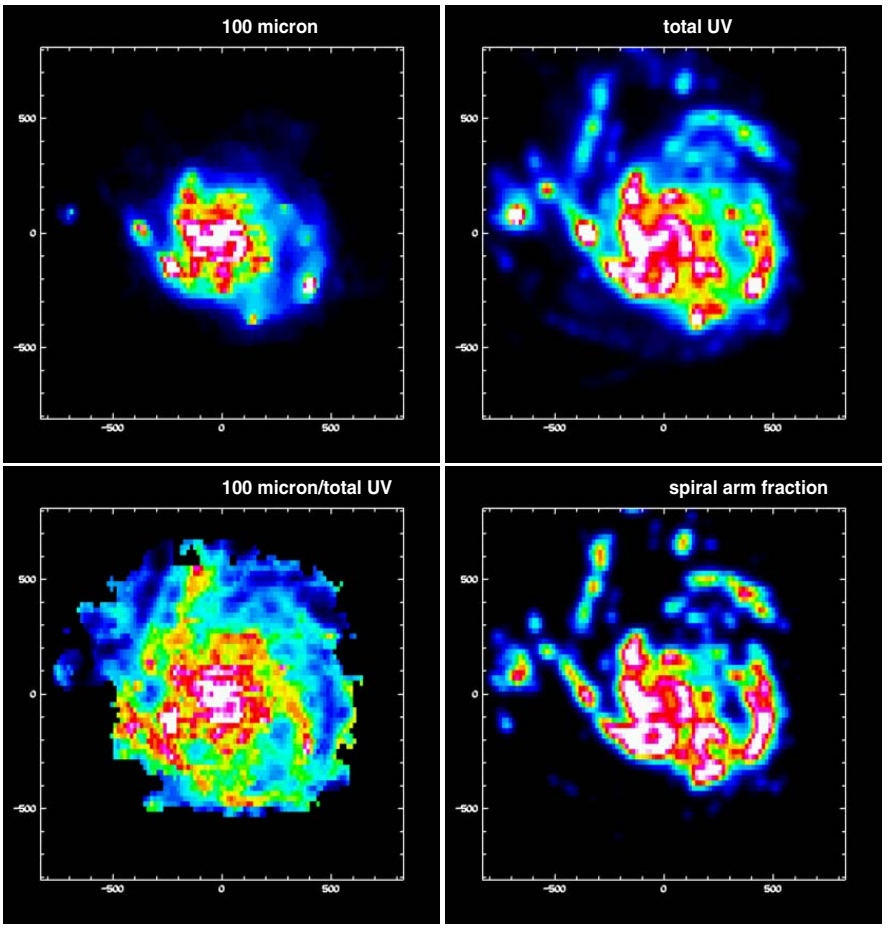

FIGURE 5. FIR-UV comparison for M 101 (Popescu et al. [72]). Top left: filter-integrated 100 μm ISOPHOT image. Top right: "total UV" image. Bottom left: ratio of the filter-integrated 100 μm ISOPHOT image divided by the corresponding "total UV" image. Bottom right: the "spiral arm fraction". All panels depict a field of $27.7' \times 27.1'$ centered at $\alpha^{2000} = 14^{\rm h}03^{\rm m}13.11^{\rm s}$; $\delta^{2000} = 54°21'06.6''$, and have the orientation, resolution and sampling ($15.33'' \times 23.00''$) of the 100 μm ISOPHOT image.

indicator of extinction in the interarm region.

Despite these local variations, the main result of Popescu et al. [72] is the discovery of a tight dependence of the FIR/UV ratio on radius, with values monotonically decreasing from ~ 4 in the nuclear region to nearly zero towards the edge of the optical disk (see Fig. 6). This was interpreted in terms of the presence of a large-scale distribution of diffuse dust having a face-on optical depth which decreases with radius and which dominates over the more localised variations in opacity between the arm and interarm regions.

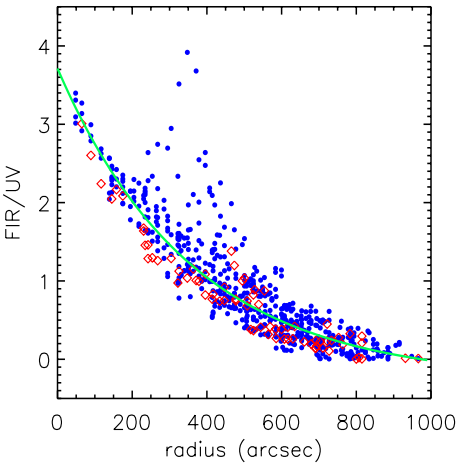

FIGURE 6. The pixel values of the FIR/UV ratio map of M 101 (Popescu et al. [72]) at the resolution of the 170 μm image versus angular radius. The blue dots are for lines of sight towards interarm regions and the red diamonds towards the spiral arm regions. The green solid line is an offset exponential fit to the data.

2.2 Integrated properties

The overriding result of all ISOPHOT studies of the integrated properties of normal galaxies in the FIR is that their SEDs in the 40-200 μm spectral range require both warm and cold dust emission components to be fitted. Although the concept of warm and cold emission components is as old as IRAS (de Jong et al. [24]), it only became possible to directly measure and spectrally separate these components using ISOPHOT's multi-filter coverage of the FIR regime out to 200 μm.

In order to investigate the integrated properties of local universe gas-rich galaxies, a number of statistical samples were constructed. All these projects were complementary in terms of selection and observational goals. In descending order of depth (measured in terms of a typical bolometric luminosity of the detected objects), the published surveys are:

The ISOPHOT Virgo Cluster Deep Survey (IVCDS; Tuffs et al. [88],[89], Popescu et al. [73]) represents the *deepest survey* (both in luminosity and surface brightness terms) of normal galaxies measured in the FIR with ISOPHOT. A complete volume- and luminosity-limited sample of 63 gas-rich Virgo Cluster galaxies selected from the Virgo Cluster Catalogue (Binggeli et al. [8]; see also Binggeli et al. [7]) with Hubble types later than S0 and brighter than $B_{\rm T} \leq 16.8$ were mapped with ISOPHOT at 60, 100 and 170 μm. The IVCDS sample was (in part) also observed with the LWS (Leech et al. [50]) and with ISOCAM (Boselli et al. [13], see also Boselli et al. [12]).

The IVCDS provides a database for statistical investigations of the FIR SEDs of gas-rich galaxies in the local universe spanning a broad range in star-formation activity and morphological types, including dwarf systems and galaxies with rather quiescent star-formation activity.

The Coma/A1367 Survey Contursi et al. [15] consists of 6 spiral and 12 irregular galaxies having IRAS detections at 60 μm. The galaxies were selected to be located within 2 or 1 degrees of the X-ray centres of Coma and A1367 clusters, respectively, with emphasis on peculiar optical morphologies. Each galaxy was observed in a single pointing with ISOPHOT, at 120, 170 and 200 μm, as well as mapped with ISOCAM in the 6.75 and 15 μm broadband filters. The sample provides a database of integrated flux densities for a pure cluster sample of high luminosity spiral and irregular galaxies.

The ISO Bright Spiral Galaxies Survey (Bendo et al. [3], [4], [5]) consists of 77 spiral and S0 galaxies chosen from the Revised Shapley-Ames Catalog (RSA), with $B_{\rm T} \leq 12.0$. Almost all are IRAS sources. Mainly an ISOCAM mapping survey with the 12 μm filter, the project also used ISOPHOT to take 60, 100 and 170 μm short stares towards the nucleus of the galaxies and towards background fields. The sample provides a database of MIR morphologies and FIR surface brightnesses of the central regions of bright spiral galaxies, including S0s.

The ISO Bright Spiral Galaxies Survey and the IVCDS represent the principle investigations of optically selected samples of normal galaxies. It should be emphasised that the main difference between them is primarily one of shallow versus deep, rather than field versus cluster, since by design the Virgo Sample predominantly consists of infalling galaxies from the field, and no cluster specific effects could be found (see also Contursi et al. [15] for Coma/A1367 Sample).

The ISO Key Project on Normal Galaxies Sample consists of 69 galaxies selected to span the whole range of the classical IRAS colour-colour diagram (Helou [36]). Since IRAS detected a vast number of galaxies in its four bands, the selection was also made to span the Hubble sequence evenly and provide a broad range of IR luminosities, dust temperatures (as determined by IRAS) and in star-formation activity. Single pointing toward the centres of the galaxies in the sample were made by ISOPHOT-S (Lu et al. [54]) to measure the 2.5-12 μm spectra and by ISOPHOT-C at 170 μm. The galaxies from this sample were also mapped with ISOCAM (Dale et al. [21]) and their main cooling lines in the FIR were measured with ISOLWS (Malhotra et al. [55]).

The ISOPHOT Serendipity Survey (Stickel et al. [81]) has initially catalogued 115 galaxies with $S_\nu \geq 2$ Jy at 170 μm and with morphological types predominantly S0/a - Scd. This sample provides a database of integrated 170 μm flux densities for relatively high luminosity spiral galaxies, all detected by IRAS at 60 & 100 μm. Recently a catalogue of 1900 galaxies was released (Stickel et al. [82]), of which a small fraction does not have IRAS detections. Most of the 1900 galaxies are spirals. The measured 170 μm flux densities range from just below 0.5 Jy up to $\sim$ 600 Jy.

2.2.1 The FIR spectral energy distribution: Dust temperatures, masses and luminosities

The presence of a cold dust emission component peaking longwards of 120 μm was inferred from studies of the integrated SEDs of individual galaxies (see Sect. 2.1.1), from statistical studies of small samples (Krügel et al. [49]; Siebenmorgen et al. [77]) and was confirmed and generalised by studies of the larger statistical samples mentioned

above. The latter studies also demonstrated the universality of the cold dust component, showing it to be present within all types of spirals (Tuffs & Popescu [87]). The cold emission component predominantly arises from dust heated by the general diffuse interstellar medium and the warm component from locally heated dust in HII regions, an interpretation consistent with what has been seen in the ISOPHOT maps of nearby galaxies (see Sect. 2.1.1) and with self-consistent modelling of the UV-FIR SEDs (see Sect. 2.3 and Popescu & Tuffs [69]).

The cold dust component is most prominent in the most "quiescent" galaxies, like those contained in the IVCD sample, where the cold dust temperatures were found to be broadly distributed, with a median of 18 K (Popescu et al. [73]), some 8 – 10 K lower than would have been predicted by IRAS. The corresponding dust masses were correspondingly found to be increased by factors of typically 2 – 10 (Stickel et al. [81]) for the Serendipity Sample and by factors 6 – 13 (Popescu et al. [73]) for the IVCD sample, with respect to previous IRAS determinations. As a consequence, the derived gas-to-dust ratios are much closer to the canonical value of ~ 160 for the Milky Way (Stickel et al. [81], Contursi et al. [15]; see also Haas et al. [34] for M 31), but with a broad distribution of values (Popescu et al. [73]).

It was found that the cold dust component provides not only the bulk of the dust masses, but even the bulk of the FIR luminosity, in particular for the case of the most quiescent spirals, like those in the IVCD sample. In contrast to the SEDs found by the other ISOPHOT studies, which typically peaked at around 170 μm, Bendo et al. [5] derived spatially integrated SEDs typically peaking at around 100 μm. The result of Bendo et al. may reflect the fact that these observations were single pointings, made towards the nucleus of resolved galaxies extending (in the main) beyond the field of view of ISOPHOT, and were therefore biased towards nuclear emission, which is warmer than the extended cold dust emission missed (or only partially covered) by these measurements. Nevertheless, the measurements of Bendo et al. constitute a useful probe of the FIR emission of the inner disks. This emission (normalised to K band emission) was found to increase along the Hubble sequence (Bendo et al. [4]).

Since the FIR carries most of the dust luminosity, it is interesting to re-evaluate the question of the fraction of stellar photons converted via grains into IR photons, taking into account the comprehensive measurements of the cold dust emission component made available by ISOPHOT. This was done by Popescu & Tuffs [66], who showed that the mean percentage of stellar light reradiated by dust is $\sim 30\%$ for the Virgo Cluster spirals contained in the IVCD sample. This study also included the dust emission radiated in the NIR-MIR range. The fact that the mean value of $\sim 30\%$ found for the Virgo Cluster spirals is the same as the canonical value obtained for the IRAS Bright Galaxy Sample (BGS; Soifer & Neugebauer [79]) is at first sight strange, since IRAS was not sensitive to the cold dust component. However the BGS sample is an IR selected sample and biased towards galaxies with higher dust luminosities, while the Virgo sample is optically selected and contain a full representation of quiescent systems. So the deficit in FIR emission caused by sample selection criteria for the Virgo sample is compensated for by the inclusion of the cold dust component. Popescu & Tuffs [66] also found evidence for an increase of the ratio of the dust emission to the total stellar emitted output along the Hubble sequence, ranging from typical values of $\sim 15\%$ for early spirals to up to $\sim 50\%$ for some late spirals. This trend was confirmed

by Boselli et al. [11] who further utilised the new ISO data on dust emission to constrain the corresponding absorption of starlight and thus improve extinction corrections (using the technique pioneered by Xu & Buat [100] for the IRAS data).

2.2.2 Two outstanding questions of the IRAS era

The radio-FIR correlation

One of the most surprising discoveries of the IRAS all-sky survey was the very tight and universal correlation between the spatially integrated FIR and radio continuum emissions (de Jong et al. [25]; Helou et al. [41]; Wunderlich et al. [99]; see Völk & Xu [94] for a review). However all the pre-ISO studies of the FIR/radio correlation were based on FIR luminosities derived from the IRAS 60 and 100 μm flux densities, and thus were missing the bulk of the cold dust luminosity. The ISOPHOT measurements at 60, 100 and 170 μm were used to redefined the FIR/radio correlation (Pierini et al. [62]) for a statistical sample of spiral galaxies. The inclusion of the cold dust component was found to produce a tendency for the total FIR/radio correlation to become more non-linear than inferred from the IRAS 60 and 100 μm observations. The use of the three FIR wavelengths also meant that, for the first time, the correlation could be directly derived for the warm and cold dust emission components.

The cold FIR/radio correlation was found to be slightly non-linear, whereas the warm FIR/radio correlation is linear. Because the effect of disk opacity in galaxies would introduce a non-linearity in the cold-FIR/radio correlation, in the opposite sense to that observed, it was argued that both the radio and the FIR emissions are likely to have a non-linear dependence on SFR. For the radio emission an enhancement of the small free-free component with SFR can account for this effect. For the cold FIR emission a detailed analysis of the dependence of local absorption and opacity of the diffuse medium on SFR is required to understand the non-linear trend of the correlation (see Pierini et al. [62]).

The improved angular resolution of ISO compared with IRAS also allowed a more detailed examination of the local FIR-radio correlation on sub-kpc size galactic sub-structures. Hippelein et al. [42] established the correlation for the star-forming regions in M 33. This correlation is shown in Fig. 7, overplotted on the correlation for integrated emission from galaxies. It is apparent that the local correlation has a shallower slope (of the order of 0.9) than for the global correlation. It was argued that the local correlation is attributable to the increase with SFR of dust absorption in increased dust densities, and to local synchrotron emission from within supernova remnants, still confining their accelerated electrons. Both emission components play only a minor role in the well known global radio-FIR correlation, that depends on the dominant large-scale absorption/re-emission properties of galaxies.

Far-infrared emission as a star-formation tracer

In the FIR, the correlation with the most widely-used star-formation tracer, Hα, is extremely non-linear, which has long led authors to suspect that the FIR emission is the result of more than one component (see e.g. Lonsdale-Persson & Helou [53]). With ISOPHOT the correlation was separately established for the warm and cold dust

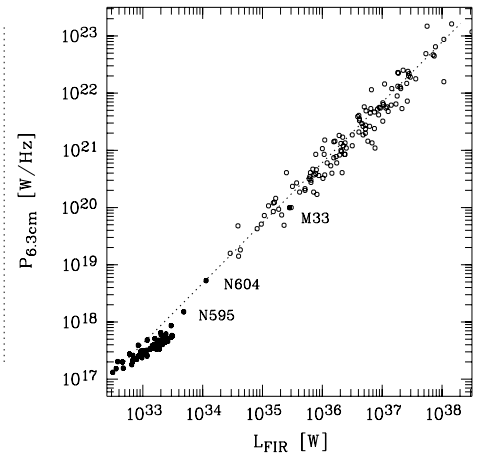

FIGURE 7. Plot of the monochromatic radio luminosity versus the FIR luminosities for M 33 (Hippelein et al. [42]) and its star-forming regions (filled circles) together with the data for the Effelsberg 100-m galaxy sample (Wunderlich et al. [99], open circle). The dotted line has a slope of 1.10 (Wunderlich & Klein [98]).

emission components. A good linear correlation was found between the warm FIR luminosities (normalised to the K band luminosity) derived for the IVCD sample and their Hα EW (Popescu et al. [73]). This is in agreement with the assumption that the warm dust component is mainly associated with dust locally heated within star-formation complexes. The scatter in the correlation was attributed to a small component of warm emission from the diffuse disk (produced either by transiently heated grains or by grains heated by the old stellar population), as well as to the likely variation in HII region dust temperatures within and between galaxies. A good but non-linear correlation was found between the cold FIR luminosities of the galaxies from the IVCD sample and their Hα EW, in the sense that FIR increases more slowly than Hα. Since the bulk of the cold FIR emission arises from the diffuse disk, the existence of this correlation implies that the grains in the diffuse disk are mainly powered by the UV photons (see also Sect. 2.3 and Popescu & Tuffs [69]). The non-linearity of the correlation is consistent with there being a higher contribution from optical photons in heating the grains in more quiescent galaxies.

For the late-type galaxies in the Coma and A1367 clusters, Contursi et al. [15] derived the relationships between the IR flux densities at 200, 170, 120, 100 and 60 μm, normalised to the H band flux, as a function of the Hα EW. It was found that the poorer correlation is in the 200 μm band and that the values of the fitted slopes decrease as the FIR wavelength increases. These results should be interpreted in terms of the increasing contribution of the diffuse component with increasing FIR wavelength.

Using the ISOPHOT observations from Tuffs et al. [88], [89] and Stickel et al. [81] in combination with UV and K band photometry, Pierini & Möller [61] have tried to quantify the effects of optical heating and disk opacity on the derivation of SFR from FIR luminosities. For this they investigated trends in the ratio of the far-IR luminosity

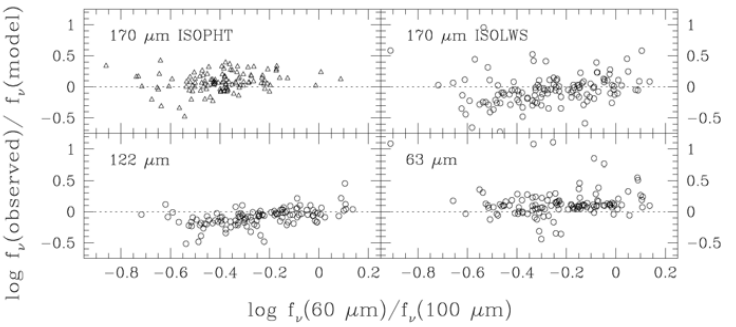

FIGURE 8. Comparison of observed FIR continuum levels observed by ISO with the model predictions of Dale & Helou [18]. The circles derive from the ISO LWS templates and the triangles represent 170 μm data from the ISOPHOT Serendipity Survey (Stickel et al. [81]).

to the intrinsic UV luminosity, L_{dust}/L_{UV}, with both disk opacity and disk mass (as measured by the intrinsic K-band luminosity). Using a separate relation between disk opacity and K band luminosity they were able re-express L_{dust}/L_{UV} in terms of a single variable, the galaxy mass. In this way they found evidence for the relative importance of optical photons in heating dust to increase with increasing galaxy mass.

2.3 Quantitative interpretation of FIR SEDs

When considered in isolation, the FIR luminosity of normal galaxies is a poor estimator of the SFR. There are two reasons for this. Firstly, these systems are only partially opaque to the UV light from young stars, exhibiting large variations in the escape probability of UV photons between different galaxies. Secondly, the optical luminosity from old stellar populations can be so large in comparison with the UV luminosity of young stellar populations that a significant fraction of the FIR luminosity can be powered by optical photons, despite the higher probability of absorption of UV photons compared to optical photons.

One step towards a quantitative interpretation of FIR SEDs was achieved by the semi-empirical models of Dale et al. [19] and Dale & Helou [18]. These authors have used ISO observations to develop a family of templates to fit the variety of the observed forms of the IR SEDs. This work assumes a power law distribution of dust masses with local radiation field intensity to provide a wide range of dust temperatures. It appears to indicate that the SEDs of star-forming galaxies can be fitted by a one-parameter family of curves (characterised by the 60/100 μm colour), determined essentially by the exponent, α, of the power law distribution of dust masses with the radiation field intensity, where the radiation field is assumed to have the colour of the local ISRF. This calibration method has been extensively used to predict FIR flux densities longwards of 100 μm for the galaxies not observed by ISOPHOT. A comparison of the FIR continuum levels observed by ISO with the Dale & Helou [18] model predictions is shown in

Fig. 8. However, a quantitative interpretation of dust emission in terms of SFRs and star-formation histories requires a combined analysis of the UV-optical/FIR-submm SEDs, embracing a self-consistent model for the propagation of the photons.

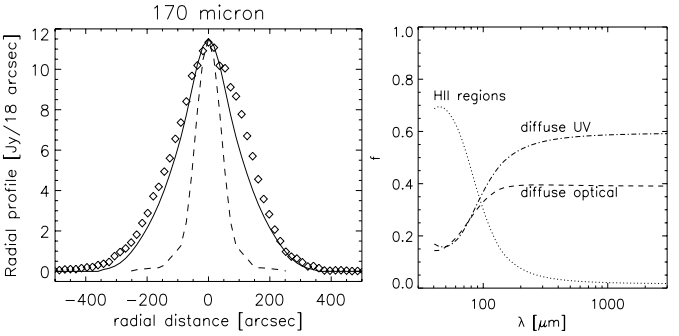

FIGURE 9. Left: The radial profile of NGC 891 at 170 μm (Popescu et al. [71]) produced by integrated the emission parallel to the minor axis of the galaxy for each bin along the major axis. Solid line: model prediction; diamonds: observed profile; dotted line: beam profile. Right: The fractional contribution of the three stellar components to the FIR emission of NGC 891 (Popescu et al. [65]).

There are a few such models in use which incorporate various geometries for the stellar populations and dust (Silva et al. [78], Bianchi et al. [6], Charlot & Fall [14], Popescu et al. [65]; see review by Popescu & Tuffs [69]). We will concentrate here on the model of Popescu et al. [65], since this is the only model which has been used to make direct predictions for the spatial distribution of the FIR emission for comparison with the ISOPHOT images. This model also ensures that the geometry of the dust and stellar populations is consistent with optical images. Full details are given by Popescu et al. [65], Misiriotis et al. [59], Popescu & Tuffs [67] and Tuffs et al. [90]. In brief, the model includes solving the radiative-transfer problem for a realistic distribution of absorbers and emitters, considering realistic models for dust, taking into account the grain-size distribution and stochastic heating of small grains and the contribution of HII regions. The FIR-submm SED is fully determined by just three parameters: the star-formation rate SFR, the dust mass $M_{\rm dust}$ associated with the young stellar population, and a factor F, defined as the fraction of non-ionising UV photons which are locally absorbed in HII regions around the massive stars. A self-consistent theoretical approach to the calculation of the F factor is given by Dopita et al. [26] in the context of modelling SEDs of starburst galaxies.

Popescu et al. [65] illustrated their model with the example of the edge-on galaxy NGC 891, which has been extensively observed at all wavelengths (including the complete submm range; Dupac et al. [27]), and also mapped with ISOPHOT at 170 and 200 μm (Popescu et al. [71]). A particularly stringent test of the model was to compare its prediction for the radial profile of the diffuse dust emission component near the peak of the FIR SED with the observed radial profiles. This comparison (Popescu et al. [71]; see also Fig. 9, left panel) showed a remarkable agreement. The excess emission in the observed profile with respect to the predicted one for the diffuse emission was explained in terms of two localised sources.

At 170 and 200 μm the model for NGC 891 predicts that the bulk of the FIR dust

emission is from the diffuse component. The close agreement between the data and the model predictions, both in integrated flux densities, but especially in terms of the spatial distribution, constitutes a strong evidence that the large-scale distribution of stellar emissivity and dust predicted by the model is in fact a good representation of NGC 891. In turn, this supports the prediction of the model that the dust emission in NGC 891 is predominantly powered by UV photons.

Depending on the FIR/submm wavelength, the UV-powered dust emission arises in different proportions from within the localised component (HII regions) and from the diffuse component (Fig. 9; right panel). For example at 60 μm, 61% of the FIR emission in NGC 891 was predicted to be powered by UV photons locally absorbed in star-forming complexes, 19% by diffuse UV photons in the weak radiation fields in the outer disk (where stochastic emission predominates), and 20% by diffuse optical photons in high energy densities in the inner part of the disk and bulge. At 100 μm the prediction was that there are approximately equal contributions from the diffuse UV, diffuse optical and locally absorbed UV photons. At 170, 200 μm and submm wavelengths, most of the dust emission in NGC 891 was predicted to be powered by the diffuse UV photons. The analysis described above does not support the preconception that the weakly heated cold dust (including the dust emitting near the peak of the SED sampled by the ISOPHOT measurements presented here) should be predominantly powered by optical rather than UV photons. The reason is as follows: the coldest grains are those which are in weaker radiation fields, either in the outer optically thin regions of the disk, or because they are shielded from radiation by optical depth effects. In the first situation the absorption probabilities of photons are controlled by the optical properties of the grains, so the UV photons will dominate the heating. The second situation arises for dust associated with the young stellar population, where the UV emissivity far exceeds the optical emissivity.

3. DWARF GALAXIES

3.1 Cold dust surrounding dwarf galaxies

Gas-rich dwarf galaxies and in particular Blue Compact Dwarfs (BCDs) were originally expected to have their FIR emission dominated by dust heated locally in HII regions. Temperatures of 30 K or more were anticipated. This was the a priori expectation in particular for the BCDs, and became the standard interpretation for the IRAS results obtained for these systems. Hoffman et al. [44], Helou et al. [37] and Melisse & Israel [57] each found that the 60/100 μm colours of BCDs were clearly warmer than those of spirals.

The IVCD Survey (Tuffs et al. [88], [89]) changed that simple picture of the FIR emission from dwarf galaxies. The IVCDS included measurements at 60, 100, and (for the first time) at 170 μm of 25 optically selected gas-rich dwarf galaxies. The observations at 60 and 100 μm were consistent with the previous IRAS results, though extending knowledge of these systems to lower luminosities. Unexpectedly however, high ratios of 170/100 μm luminosities were found in many of the surveyed systems. Such long-wavelength excesses were found both in relatively high-luminosity dwarfs,

such as VCC655, as well as in fainter objects near the limiting sensitivity of the survey. These observations imply the presence of large amounts of cold dust.

As shown by Popescu et al. [73], it seems unlikely that the cold dust resides in the optically thick molecular component associated with star-formation regions, since the implied dust masses would be up to an order of magnitude greater than those typically found in giant spirals. Such large masses could not have been produced through star-formation within the dwarfs over their lifetime. One alternative is that the dust originates and still resides outside the optical extent of these galaxies. In fact, some evidence for this was provided by the ISOPHOT observations themselves, since they were made in the form of scan maps, from which estimates of source sizes could be determined. Even with the relatively coarse beam ($1.6'$ FWHM at $170\,\mu$m), the extended nature of the sources could be clearly seen in a few cases for which the FWHM for the $170\,\mu$m emission exceeds the optical diameters of the galaxies (to 25.5Bmag/arcsec^2) by factors of between 1.5 and 3.5. It is interesting to note that two of these galaxies (VCC 848 and VCC 81) have also been mapped in HI (Hoffman et al. [45]), revealing neutral hydrogen sizes comparable to the $170\,\mu$m extent. This raises the possibility that the cold dust is embedded in the extended HI gas, external to the optical galaxy. This would be analogous to the case of the edge-on spiral NGC 891, where Popescu & Tuffs [68] discovered a cold-dust counterpart to the extended HI disk (see Sect. 2.1.2). In this context the main observational difference between the giant spiral and the dwarfs may be that for the dwarfs the integrated $170\,\mu$m emission is dominated by the extended emission component external to the main optical body of the galaxy, whereas for the giant spirals the long-wavelength emission predominantly arises from within the confines of the optical disk of the galaxy.

Apart from the SMC (which is discussed in Sect. 3.2 and is too extended for ISOPHOT to map beyond its optical extent), only three dwarf galaxies were observed by ISOPHOT in the field environment (all Serendipity Survey sources; Stickel et al. [81]). All three sources have comparable flux densities at 100 and $170\,\mu$m. But the small statistics mean that it is still an open question to which extent the cold dust emission associated with the extended HI component in dwarf galaxies is a cluster phenomenon or not. Of potential relevance to the origin of the dust seen surrounding Virgo dwarfs is the discovery by ISOPHOT of the source "M 86-FIR" in the halo of M 86 (Stickel et al. [80]) which has no optical counterpart. It may be a "relic" ISM stripped from a spiral galaxy in the Virgo Cluster.

The existence of large quantities of dust surrounding gas-rich dwarf galaxies may have important implications for our understanding of the distant Universe. According to the hierarchical galaxy formation scenarios, gas-rich dwarf galaxies should prevail at the earliest epochs. We would then expect these same galaxies to make a higher contribution to the total FIR output in the early Universe, certainly more than previously expected.

3.2 Infrared emission from within dwarf galaxies

The distribution of cold dust within dwarf galaxies could be studied in only one case, namely in the resolved ($1.5'$ resolution) $170\,\mu$m ISOPHOT map of the Small

Magellanic Cloud (Wilke et al. [97], [96]). The 170 μm ISO map of the SMC reveals a wealth of structure, not only consisting of filamentary FIR emitting regions, but also of numerous (243 in total) bright sources which trace the bar along its major axis as well as the bridge which connects the SMC to the LMC. Most of the brighter sources have cold components, associated with molecular clouds. The discrete sources were found to contribute 28%, 29% and 36% to the integrated flux densities at 60, 100 and 170 μm, respectively. The SED was modelled by the superposition of 45 K, 20.5 K and 10 K blackbody components with emissivity index β=2. The average dust colour temperature (averaged over all pixels of the 170/100 colour map) was found to be $T_{\rm D} = 20.3$ K.

Bot et al. [9] have compared the FIR map of the SMC with an HI map of similar resolution. This reveals a good spatial correlation of the two emissions in the diffuse regions of the maps (regions that fall outside of the correlation are either hot star-forming regions, or cold molecular clouds with no associated HI). Adding the IRAS data allows them to compute the FIR emissivity per unit H atom. Bot et al. [9] found that this emissivity is lower than in the Milky Way, and in fact it is even lower than the lower metallicity ($Z_{\odot}/10$) of the SMC would imply, suggesting that depletion mechanisms at work in the ISM have more than a linear dependence on metallicity.

Although FIR emission from dwarf galaxies has been associated only with gas-rich dwarfs, in one particular case such emission has been detected in a dwarf elliptical galaxy, as well. This is the case of NGC 205, one of the companions of M 31, classified as a peculiar dE5. This galaxy shows signatures of recent star-formation (Hodge [43]) and of extended HI emission (Young & Lo [101]), and was detected by IRAS (Rice et al. [74], Knapp et al. [48], with a SED steeply rising between 60 and 100 μm. Based on ISOPHOT observations, Haas [34] showed that the FIR emission is resolved and similar to that seen in HI. He also presented evidence for a very cold dust component, of 10 K, coming from the center of the galaxy.

Galliano et al. [30] modelled the UV-optical/MIR-FIR-submm SED of the low metallicity nearby dwarf galaxy NGC1569. (Fig. 10). This study is noteworthy in that it constrains the grain size distribution through the MIR-FIR ISOCAM and ISOPHOT observations and therefore gives more specific information about grain properties in dwarf galaxies. The results indicate a paucity of Polycyclic Aromatic Hydrocarbons (PAHs) due to an enhanced destruction in the intense ambient UV radiation field, as well as an overabundance (compared to Milky Way type dust) of small grains of size ~ 3 nm, possibly indicative of a redistribution of grain sizes through the effect of shocks.

4. CONCLUSIONS AND OUTLOOK

ISOPHOT has not only advanced the knowledge of IR properties of normal galaxies but has also made unexpected discoveries. The bulk of the emission from dust has been measured, revealing cold dust in copious quantities. This dust is present in all types of normal galaxies and is predominantly distributed in a diffuse disk with an intrinsic scalelength exceeding that of the stars. Cold dust has been found beyond the optical regions of isolated galaxies, associated with the extended HI disks of spiral galaxies or with the HI envelopes of dwarf galaxies. The fraction of the bolometric luminosity

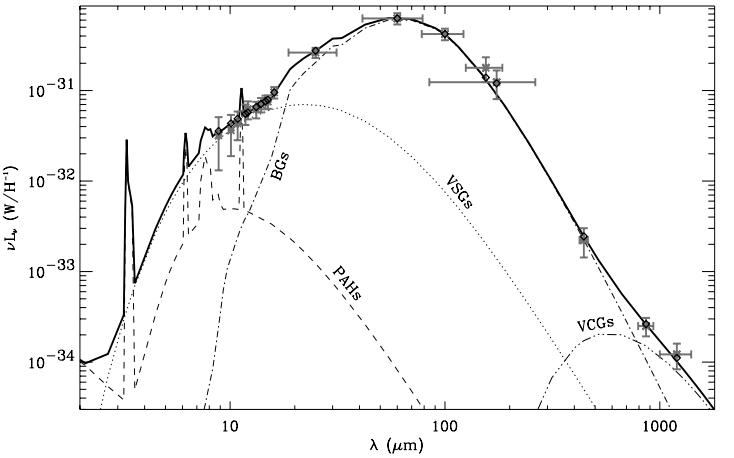

FIGURE 10. NGC 1569 observations and modeled SED from Galliano et al. [30]. The data are indicated by crosses: vertical bars are the errors on the flux density values and the horizontal bars indicate the widths of the broadbands. The lines show the predictions of the dust model with its different components. Diamonds indicate the model predictions integrated over the observational broadbands and colour-corrected.

radiated by dust has been measured for the first time. Realistic geometries for stars and dust have been derived from ISOPHOT imaging observations, enabling the contribution of the various stellar populations to the dust heating to be accurately derived. This enormous advancement in the understanding of normal galaxies in the nearby Universe has laid the foundation for more detailed investigations with Spitzer and Herschel. A clear priority is to increase the number of galaxies with detailed imaging information and to provide better statistics on carefully selected samples, especially those selected in the optical/NIR bands. Ultimately, the improved sensitivity of the new infrared space observatories will allow knowledge of the dust emission from normal galaxies to be extended beyond the nearby universe.

ACKNOWLEDGMENTS

The authors would like to take this opportunity to thank all the individuals that helped make the ISO mission a success. R.J. Tuffs and C.C. Popescu would also like to thank Heinrich J. Völk for enlightening discussions.

REFERENCES

1. Alton P.B., Bianchi S., Rand R.J., Xilouris, E.M., Davies, J.I. et al., 1998b, ApJ, 507, L125
2. Alton, P.B., Trewhella, M., Davies, J.I., Evans, R., Bianchi, S., et al. 1998a, A&A, 335, 807

3. Bendo, G.J., Joseph, R.D., Wells, M., Gallais, P., Haas, M. et al. 2002a, AJ 123, 3067
4. Bendo, G.J., Joseph, R.D., Wells, M., Gallais, P., Haas, M. et al. 2002b, AJ 124, 1380
5. Bendo, G.J., Joseph, R.D., Wells, M., Gallais, P., Haas, M. et al. 2003, AJ 125, 2361
6. Bianchi, S., Davies, J. I., Alton, P. B. 2000, A&A 359, 65
7. Binggeli, B., Popescu, C.C. & Tammann, G.A. 1993, A&AS, 98, 275
8. Binggeli, B., Sandage, A. & Tammann, G.A. 1985, AJ, 90, 1681
9. Bot, C., Boulanger, F., Lagache, G., Cambrésy, L., Egret, D. 2004 A&A 423, 567
10. Boselli, A., Gavazzi, G., Lequeux, J. Pierini, D. 2002, A&A 385, 454
11. Boselli, A., Gavazzi, G., Sanvito, G. 2003a, A&A 402, 37
12. Boselli, A., Lequeux, J., Contursi, A. Gavazzi, G., Boulade, O., et al. 1997, A&A, 324, L13
13. Boselli, A., Sauvage, M., Lequeux, J., Donati, A, & Gavazzi, G. 2003b, A&A 406, 867
14. Charlot, S., & Fall, S.M. 2000, ApJ 539, 718
15. Contursi, A., Boselli, A., Gavazzi, G., Bertagna, E., Tuffs, R., Lequeux, J. 2001, A&A 365, 11
16. Contursi, A., Lequeux, J., Hanus, M., Heydari-Malayeri, M., Bonoli, C., Bosma, A., et al. 1998, A&A 336, 662
17. Contursi, A., Lequeux, J., Cesarsky, D., Boulanger, F., Rubio, M., Hanus, M. et al. 2000, A&A 362, 310
18. Dale, D. & Helou, G. 2002, ApJ 576, 159
19. Dale, D. A., Helou, G., Contursi, A., Silbermann, N. A. & Kolhatkar, S. 2001, ApJ, 549, 215
20. Dale, D. A., Helou, G., Silbermann, N. A., Contursi, A., Malhotra, S., Rubin, R. H. 1999, AJ 118, 2055
21. Dale, D. A., Silbermann, N. A., Helou, G., Valjavec, E., Malhotra, S., Beichmann, C. A., et al. 2000, AJ 120, 583
22. Davies, J. I., Alton, P., Bianchi, S. & Trewhella, M. 1998, MNRAS 300, 1006
23. Davies, J.I., Alton, P., Trewhella, M., Evans, R., & Bianchi, S. 1999, MNRAS, 304, 495
24. de Jong, T., Clegg, P.E., Soifer, B.T.., et al. 1984, ApJ, 278, L67
25. de Jong, T., Klein, U., Wielebinski, R., Wunderlich, E. 1985, A&A, 147, L6
26. Dopita, M.A., Groves, B.A., Fischera, J., Sutherland, R.S., Tuffs, R.J. et al. 2005, ApJ, in press
27. Dupac, X., del Burgo, C., Bernard, J.-P., et al. 2003, MNRAS 344, 105
28. Ferguson, A., Gallagher, J.S. & Wyse, R. 1998, AJ 116, 673
29. Ferrara, A., Ferrini, F., Barsella, B., & Franco, J. 1991, ApJ 381, 137
30. Galliano, F., Madden, S.C., Jones, A.P., Wilson, C.D., Bernard, J.-P., et al. 2003, A&A 407, 159
31. Gerhard, O. & Silk, J. 1996, ApJ 472, 34
34. Haas, M. 1998, A&A 337, L1
33. Haas, M., Klaas, U., Bianchi, S. 2002, A&A 385, L23
34. Haas, M., Lemke, D., Stickel, M., Hippelein, H., Kunkel, M. et al. 1998, A&A, 338, L33
35. Haas, M., Siebenmorgen, R., Leipski, C., Ott, S., Cunow, B., Meusinger, H., et al. 2004, A&A 419, L49
36. Helou, G. 1986, ApJ 311, 33
37. Helou, G., Khan, I. R., Malek, L., & Boehmer, L. 1988, ApJS, 68, 151
38. Helou, G., Malhotra, S., Beichman, C. A., Dinerstein, H., Hollenbach, D. J., Hunter, D. A., et al. 1996, A&A 315, L157
39. Helou, G., Malhotra, S., Hollenbach, D. J., Dale, D. A., Contursi, A. 2001, ApJ 548, L73
40. Helou, G., Roussel, H., Appleton, P., Frayer, D., Stolovy, S., et al. 2004, ApJS, in press
41. Helou, G., Soifer, B. T., & Rowan-Robinson, M. R. 1985, ApJ, 298, L7
42. Hippelein, H., Haas, M., Tuffs, R.J., Lemke, D., Stickel, M. et al. 2003, A&A 407, 137
43. Hodge, P. 1973, ApJ 182, 671
44. Hoffman, G. L., Helou, G., Salpeter, E. E., Lewis, B. M. 1989, ApJ, 339, 812
45. Hoffman, G. L., Salpeter, E. E., Farhat, B., Roos, T., Williams, H., and Helou, G. 1996, ApJS 105, 269
46. Hunter, D. A., Kaufman, M., Hollenbach, D. J., Rubin, R. H., Malhotra, S., et al. 2001, ApJ 553, 121
47. Kessler, M. F., Steinz, J. A., Anderegg, M. E., Clavel, J., Drechsel, G., et al. 1996, A&A, 315, 27
48. Knapp, G.R., Guhathakurta, P., Kin, D.W., Jura, M. 1989, ApJS 70, 329
49. Krügel, E., Siebenmorgen, R., Zota, V., Chini, R. 1998, A&A, 331, L9
50. Leech, K.J., Völk, H.J., Heinrichsen, I., Hippelein, H., Metcalfe, L., et al. 1999, MNRAS, 310, 317
51. Lemke, D., Klaas, U., Abolins, J., Ábráham, P., Acosta-Pulido, J., et al. 1996, A&A, 315, L64

52. Li, A., Draine, B. T. 2002, ApJ 572, 232
53. Lonsdale-Persson C. J., Helou, G. 1987, ApJ 314, 513
54. Lu, N., Helou, G., Werner, M. W., Dinerstein, H. L., Dale, D. A., et al. 2003, ApJ 588, 199
55. Malhotra, S., Kaufman, M.J., Hollenbach, D., Helou, G., Rubin, R.H. et al. 2001, ApJ 561, 766
56. Martin, C. et al. 2005, ApJ Letters, in press
57. Melisse, J. P. M., Israel, F. P. 1994, A&A, 285, 51
58. Meijerink, R., Tilanus, R.P.J., Dullemond, C.P., Israel, F.P., & van der Werf, P.P. 2004, A&A in press
59. Misiriotis A., Popescu, C.C., Tuffs, R.J., & Kylafis, N.D. 2001, A&A, 372, 775
60. Pierini, D., Leech, K. J., Völk, H. J. 2003a, A&A, 397, 871
61. Pierini, D. & Möller, C. 2003, MNRAS 346, 818
62. Pierini, D., Popescu, C. C., Tuffs, R. J., Völk, H. J. 2003b, A&A 409, 907
63. Pfenniger, D., Combes, F. 1994, A&A 285, 94
64. Pfenniger, D., Combes, F., Martinet, L. 1994, A&A 285, 79
65. Popescu, C.C., Misiriotis A., Kylafis, N.D., Tuffs, R.J., & Fischera, J., 2000b, A&A, 362, 138
66. Popescu, C.C., Tuffs, R.J. 2002a, MNRAS 335, L41
67. Popescu, C.C., Tuffs, R.J. 2002b, Reviews in Modern Astronomy, vol 15., Edited by Reinhard E. Schielicke. Wiley, ISBN 352640404X, p.239
68. Popescu, C.C, Tuffs, R.J. 2003, A&A 410, L21
69. Popescu, C.C, Tuffs, R.J. 2005, in "The Spectral Energy Distribution of Gas-Rich Galaxies: Confronting Models with Data", Heidelberg, 4-8 Oct. 2004, eds. C.C. Popescu & R.J. Tuffs, AIP Conf. Ser., in press
70. Popescu, C.C., Tuffs, R.J., Fischera, J., Völk, H.J. 2000a, A&A, 354, 480
71. Popescu, C. C., Tuffs, R. J., Kylafis, N. D. & Madore, B. F. 2004, A&A 414, 45
72. Popescu, C.C., Tuffs, R.J., Madore, B.F., Gil de Paz, A., Völk, H. et al. 2005, ApJ 619, L75
73. Popescu, C.C., Tuffs, R.J., Völk, H.J., Pierini, D. & Madore, B.F., 2002, ApJ 567, 221
74. Rice, W., Lonsdale, C.J., & Soifer, B.T., et al. 1988, ApJS 68, 91
75. Roussel, H., Vigroux, L., Bosma, A., Sauvage, M., Bonoli, C., Gallais, P., et al. 2001c, A&A 369, 473
76. Schmidtobreick, L., Haas, M., & Lemke, D. 2000, A&A 363, 917
77. Siebenmorgen, R., Krügel, E., Chini, R. 1999, A&A, 351, 495
78. Silva, L., Granato, G. L., Bressan, A., Danese, L. 1998, ApJ 509, 103
79. Soifer, B.T., & Neugebauer, G. 1991, AJ, 101, 354
80. Stickel, M., Bregman, J.N., Fabian, A.C., White, D.A., & Elmegreen, D.M. 2003, A&A 397, 503
81. Stickel, M., Lemke, D., Klaas, U., Beichman, C.A., Rowan-Robinson, M. et al. 2000, A&A 359, 865
82. Stickel, M., Lemke, D., Klaas, U., Krause, O., & Egner, S. 2004, A&A 422, 39
83. Swaters, R. A., Sancisi, R. & van der Hulst, J. M. 1997, ApJ 491, 140
84. Trewhella, M., Davies, J. I., Alton, P. B., Bianchi, S., & Madore, B. F. 2000, ApJ 543, 153
85. Tuffs, R.J., Lemke, D., Xu, C. et al. 1996, A&A 315, L149
86. Tuffs, R.J. & Gabriel, C., 2003, A&A 410, 1075
87. Tuffs, R.J. & Popescu, C.C. 2003, in "Exploiting the ISO Data Archive. Infrared Astronomy in the Internet Age", Siguenza, Spain 24-27 June, 2002. Eds. C. Gry et al., ESA SP-511, p. 239.
88. Tuffs, R.J., Popescu, C.C., Pierini, D., Völk, H. J., Hippelein, H. et al. 2002a, ApJS 139, 37
89. Tuffs, R.J., Popescu, C.C., Pierini, D., Völk, H. J., Hippelein, H. et al. 2002b, ApJS 140, 609
90. Tuffs, R.J., Popescu, C. C., Völk, H.J., Kylafis, N.D., & Dopita, M.A. 2004, A&A 419, 821
91. Valentijn, E. A., van der Werf, P. P. 1999a, in Proceedings of the Conference "The Universe as seem by ISO", Eds. P. Cox & M. F. Kessler. ESA-SP 427., p.821
92. Valentijn, E. A. & van der Werf, P. P. 1999b, ApJ 522, L29
93. Valentijn, E. A., van der Werf, P. P., de Graauw, Th., de Jong, T. 1996, A&A 315, L145
94. Völk, H.J., & Xu, C. 1994, Infrared Physics and Technology, 35, 527
95. Walsh, W., Beck, R., Thuma, G., et al. 2002, A&A 388, 7
96. Wilke, K., Klaas, U., Lemke, D., Mattila, K., Stickel, M., et al. 2004, A&A 414, 69
97. Wilke, K., Stickel, M., Haas, M., Herbstmeier, U., Klaas, U., et al. 2003, A&A 401, 873
98. Wunderlich, E., Klein, U. 1988, A&A 206, 47
99. Wunderlich, E., Wielebinski, R. & Klein, U. 1987, A&AS 69, 487
100. Xu, C. & Buat, V. 1995, A&A 293, L65
101. Young, L.M. & Lo, K.Y. 1997, ApJ 476, 131